Carbon Nanotube Chirality Determines Efficiency of Electron Transfer to Fullerene in All-Carbon Photovoltaics

ARTICLE *in* JOURNAL OF PHYSICAL CHEMISTRY LETTERS · AUGUST 2013

Impact Factor: 7.46 · DOI: 10.1021/jz401369s

THE JOURNAL OF PHYSICAL CHEMISTRY Letters

Letter

pubs.acs.org/JPCL

Carbon Nanotube Chirality Determines Efficiency of Electron Transfer to Fullerene in All-Carbon Photovoltaics

Christine M. Isborn,*[,†] Chun Tang,[§] Ashlie Martini,[§] Erin R. Johnson,[†] Alberto Otero-de-la-Roza,[†] and Vincent C. Tung*[,‡]

[†]Chemistry and Chemical Biology, University of California, Merced, California 95343, United States

[‡]Materials Engineering, University of California, Merced, California 95343, United States

[§]Mechanical Engineering, University of California, Merced, California 95343, United States

Supporting Information

ABSTRACT: Nanocarbon-based photovoltaics offer a promising new architecture for the next generation of solar cells. We demonstrate that a key factor determining the efficiency of single-walled carbon nanotube (SWCNT)/fullerene devices is the chirality of the SWCNT. This is shown via current density vs voltage measurements of nanocarbon devices prepared with (9,7), (7,6) and (6,5) SWCNTs, as well as density-functional theory (DFT) density of states calculations of C_{60} adsorbed onto the corresponding SWCNTs. The trends in efficiency are rationalized in terms of the relative energies of the fullerene and SWCNT conduction band energy levels.

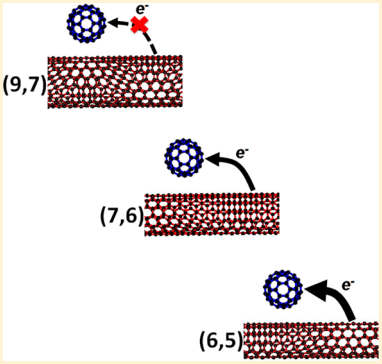

SECTION: Physical Processes in Nanomaterials and Nanostructures

The development of affordable photovoltaic technologies, i.e., solar cells, offers a promising long-term solution for clean, renewable energy.[1] Because the dielectric constant of organic materials is low compared to inorganic semiconductors, optical excitation in organic materials gives rise to a strongly bound electron−hole pair, called an exciton, rather than free charge carriers.[2] Organic-materials-based photovoltaics thus face the additional challenge of separating the Coulombically attracted electron and hole. If a compound near the exciton has a high enough electron affinity, this compound can act as an electron acceptor. The energy gained via this electron transfer must exceed the exciton binding energy.

A new organic material architecture for photovoltaics is all-carbon-based nanomaterials composed of electron-accepting fullerenes and electron-donating single-walled carbon nanotubes (SWCNTs).[3−11] A SWCNT can be thought of as a wrapped graphene sheet, with the type of wrapping determining the diameter and chirality of the SWCNT, as labeled by the indices (n,m).[10,12] The SWCNTs can be either metallic or semiconducting, with both types having excellent charge transport properties. Synthesis of SWCNTs in reasonable quantities leads to a broad mixture of chiralities, and generally includes both metallic and semiconducting SWCNTs. However, recent advances in SWCNT separation techniques have enabled the purification of SWCNTs into samples dominated by a single SWCNT chirality. Our work herein demonstrates that, with the proper choice of SWCNT, a fullerene-SWCNT-graphene nanoribbon hybrid can efficiently harness photogenerated charge carriers. Upon exciton generation, the functional heterojunction enables exciton separation when the electron is transferred from the SWCNT donor to the fullerene acceptor.

Because they have low-energy conduction band levels and small electron-transfer reorganization energy due to their constrained structure and delocalized π system, fullerenes are established electron acceptors.[12−16] They are a common component of bulk-heterojunction polymeric photovoltaic materials. However, in these disordered systems, it has been difficult to optimize the size of the donor(polymer)−acceptor-(fullerene) domain to facilitate charge separation before electron−hole recombination.[17−20] For the all-carbon photovoltaics studied herein, the fullerenes surround the outside of the SWCNT (see Scheme 1). This arrangement has two advantages: (1) the adsorbed fullerenes remain close to the SWCNT via $\pi-\pi$ stacking interactions, providing a short diffusion length for the electron transfer upon optical excitation of the SWCNT, and (2) there is no covalent bonding of the electron donor and acceptor materials that will disturb their electronic properties. The fullerene−SWCNT system prepared in this work additionally includes a graphene nanoribbon (GNR) wrapper to stabilize the tubular heterostructure. Graphene is optically transparent (transmittance of 97.7%[21]),

Received: July 2, 2013
Accepted: August 9, 2013

   dx.doi.org/10.1021/jz401369s | J. Phys. Chem. Lett. 2013, 4, 2914−2918

Scheme 1. SWCNT/C_{60} Stabilized by Graphene Nanoribbon Wrapping

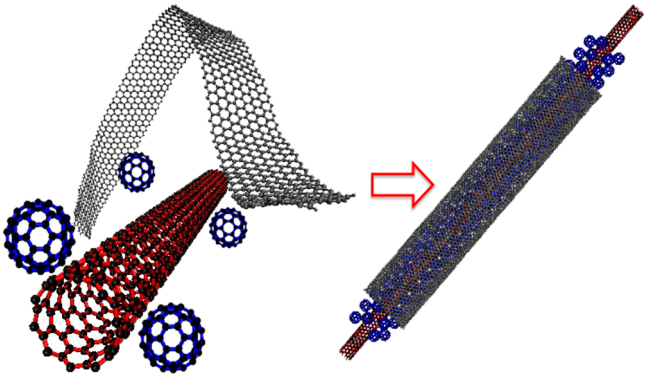

and has a high mobility for both electrons and holes. The specific structural and energetic effects of the GNR in this heterostructure will be the subject of future work.

We present here experimental evidence supported by density-functional theory (DFT) electronic structure calculations showing that the SWCNT chirality determines the efficiency of the electron transfer at the fullerene-SWCNT junction. Our work shows that choosing the optimum SWCNT chirality will be key to improving the efficiency of nanocarbon-based photovoltaic cells. Hybrid systems of (9,7), (7,6), and (6,5) semiconducting SWCNT chiralities were characterized in terms of their efficiency using current–voltage measurements. The density of states computed with DFT gives insight into the relative energy levels of these materials, and rationalizes the energetic driving force for electron transfer in terms of the relative energies of the conduction bands of the fullerene and SWCNTs.

The synthesis of the GNRs followed an approach from the literature for unzipping multiwalled CNTs (MWCNTs) with selected diameters.[22,23] Details of the solution processed, self-ordering core–shell composite synthesis and accompanying atomic force microscopy image (see Figure S1) can be found in the Supporting Information (SI). The colloidal dispersion of core–shell SWCNT/C_{60}/GNR heterostructures in a mixture of deionized-water and methanol in a volume ratio of 9 to 1 was found to remain stable for months without visible precipitation and can be readily spin-coated onto a wide variety of substrates for characterization.

In our previous work,[24] we found that the effectiveness of the GNR wrap depends on aspect ratio and that a 100 to 1 ratio is ideal in terms of optimizing structural stability without forming graphite-like walls which adversely affect the overall photoresponse. The all-carbon composite core–shell structures were characterized by high-resolution scanning and transmission electron microscopy and the unique core–shell conformation remained intact even after high temperature annealing (>300 °C) and prolonged measurement in aqueous medium.[24]

In this study we evaluate the photovoltaic performance of the all-carbon composite material. Porous networks comprised of C_{60}/SWCNTs/GNRs were electro-spray coated into a 7–10 nm active layer on indium tin oxide (ITO) substrates precoated with a modification layer of graphene oxide and acid-treated SWCNTs (GO:SWCNT). Thin films of GO:SWCNT are known[25−27] to provide preferred energetics and improved vertical transport characteristics, surpassing the commonly used hole transporting layer, poly(3,4-ethylenedioxythiophene):poly(styrenesulfonate) (PEDOT:PSS). Figure 1a shows the device structure. Thermal annealing at 150 °C for 30 min was found to be sufficient to establish the conductive pathways across the carbon–carbon junctions. Next, a 45 nm layer of PCBM was spin-coated onto the all-carbon composite film. This PCBM layer acts as a smoothing and blocking layer to prevent shorting, as an electron-transporting layer, and as an additional absorber in the 350–500 nm range. To further improve electron transport and suppress the possibility of recombination, a thin layer of ZnO nanoparticles (5 mg/mL in ethanol) was spin-cast on top of the PCBM blocking layer. Finally, 100 nm of Ca:Al electrodes were thermally evaporated to complete the device.

The output current–voltage (J–V) characteristics of representative devices for the three SWCNT chiralities are depicted in Figure 1b. All devices exhibit a pronounced photovoltaic response. In particular, devices made of (6,5) and (7,6) chirality SWCNTs are significantly more responsive than those made of (9,7), with (6,5) having a power conversion efficiency (PCE) readily surpassing 1%, see Table 1. Values are given for the open-circuit voltage (V_{OC}), the short-circuit current density (J_{SC}) in mA/cm^2, and the fill factor (FF).

To determine how efficiently incident photons of various wavelengths are converted to electrons, the incident photon-to-current efficiency (IPCE), also termed the external quantum efficiency (EQE), was measured for the C_{60}/(6,5) SWCNT/GNR device (see Figure 2a). The efficiency is fairly high in the

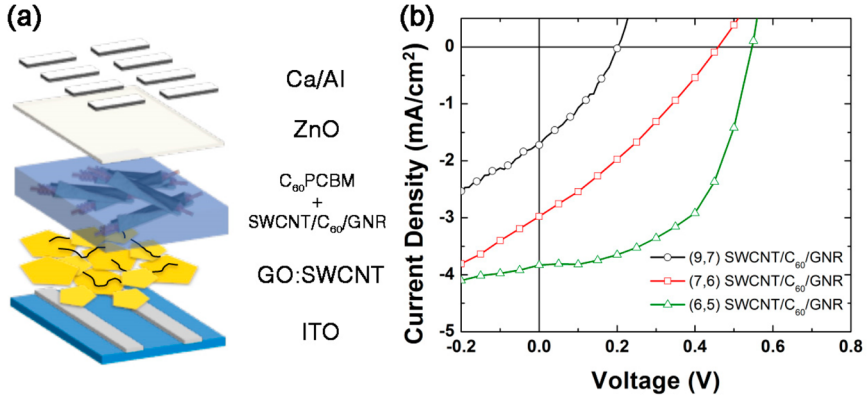

Figure 1. (a) Schematic illustration of device structure using the C_{60}/SWCNTs/GNR composite as the active layer. (b) Chirality dependent current–voltage (J–V) characteristics of the all-carbon photovoltaic cells.

dx.doi.org/10.1021/jz401369s | J. Phys. Chem. Lett. 2013, 4, 2914–2918

Table 1. Photocurrent Measurements for Nanocarbon Devices with the Three SWCNT Chiralities

SWCNT	V_{OC} (V)	J_{SC} (mA/cm^2)	FF	PCE (%)
(9,7)	0.21	1.72	0.33	0.12
(7,6)	0.45	2.97	0.32	0.42
(6,5)	0.55	3.83	0.55	1.14

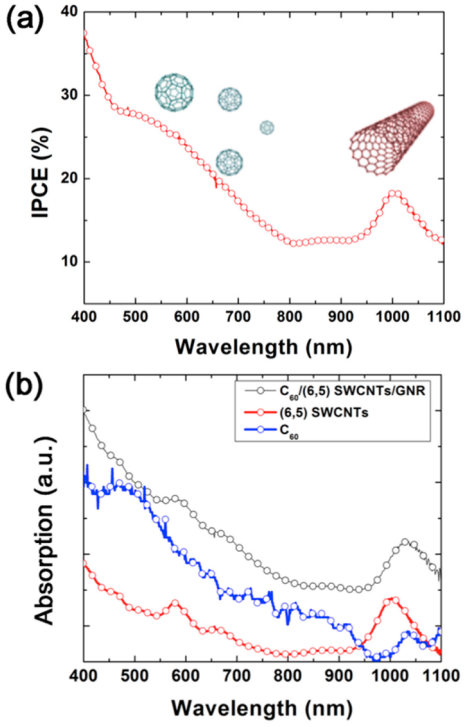

Figure 2. (a) IPCE measurement for the C_{60}/(6,5) SWCNT/GNR device. (b) Absorption spectra of C_{60} (blue), (6,5) SWCNTs (red), and the C_{60}/(6,5)SWCNT/GNR composite (black).

visible region (20−30%) and the peak in the low-energy region near 1000 nm is in good agreement with the peak in the absorption spectrum for (6,5) SWCNTs (Figure 2b), indicating that optical excitation of the SWCNT is the primary source of electrons for the photocurrent in this energy range. We also tested the device performance without the PCBM layer (see Figure S2) and found a decreased fill factor and also decreased absorption in the 350−500 nm range. This decreases the PCE of the (6,5) SWCNT device from 1.14% to 0.45%. The PCBM layer thus not only helps to improve the junction quality, but also provides increased photoresponse at higher energies.

We attribute the high efficiency of these all-carbon composite devices to the well-defined geometry and chirality of these heterostructures and to the relative energetics of the active constituents (described below). The GNR wrapper ensures close contact between the C_{60} electron acceptor and SWCNT donor throughout the active layer, providing many sites for charge separation to occur upon exciton generation. By using only one chirality of semiconducting SWCNT rather than a mixture of SWCNTs, the energetics are well-defined and there is no exciton quenching and shorting by metallic nanotubes.

The energies of the edge of the valence band of various device components were experimentally determined by ultraviolet photoelectron spectroscopy (UPS); these values are shown below the representative material in Figure 3. The energy values shown above the material are estimates of the

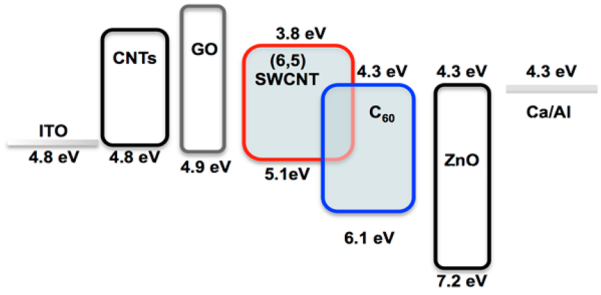

Figure 3. Schematic energy level diagram of nanocarbon device based on UPS values for the valence band, and UV/vis spectra for the band gap and corresponding conduction band.

energy of the conduction band edge based on UV/vis absorption spectra. The energetically aligned energy levels between C_{60} and the (6,5) SWCNT facilitate efficient exciton dissociation and subsequent carrier transportation in the device. However, in the cases of (9,7) and (7,6) SWCNT/C_{60} assemblies, the combination of a relatively small driving force for exciton dissociation and unfavorable energetic routes for hole transport collectively result in poor photovoltaic response[28] (see Figure S3 for (9,7) and (7,6) energy schematics). If photogenerated excitons can be dissociated at the SWCNT/C_{60} interfaces, as with the (6,5) assembly, holes will propagate through the backbone of the SWCNTs because of the 1-D like structure. Electrons will be transported through energetically favorable pathways established by fullerene shells, GNR networks, and PCBM. Thin layers of wide band gap ZnO nanoparticles provide an energetic barrier to inhibit unwanted charge recombination.

To further interpret the advantageous structural and electronic features of our all-carbon tubular assembly, we turn to a combination of classical molecular dynamics and DFT. Molecular dynamics were used to create an atomistic model of the SWCNT/C_{60}/GNR systems. Thirty-six C_{60} molecules were placed in a hexagonal-close-packed pattern surrounding the SWCNT surface. A 144 × 40 Å^2 GNR was placed near the SWCNT/C_{60} structure, and then dynamics were run at 300 K for 1 ns using the AIREBO potential[29] and the Nosé−Hoover thermostat in the LAMMPS molecular dynamics package (http://lammps.sandia.gov).[30] The GNR wrapped around the C_{60}-coated SWCNT forming a multicore−shell structure (see Scheme 1). Figure 4a shows an axial view of the structure. The subset used in the DFT band structure calculations is indicated by a dashed rectangle, and is shown in detail in Figure 4b. The SWCNT is represented by a 16 Å-long section terminated with

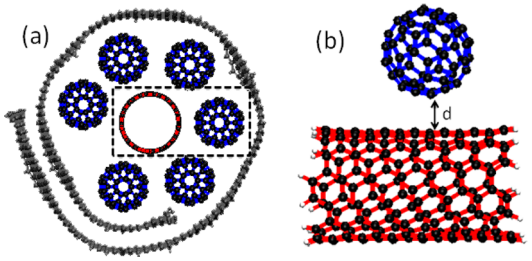

Figure 4. (a) Snapshot of the atomistic model along the axis direction with a dashed-line indicating the region included in the DFT calculations. (b) The DFT region shown in detail, where d is the C_{60}-SWCNT distance of 3 Å.

dx.doi.org/10.1021/jz401369s | J. Phys. Chem. Lett. 2013, 4, 2914−2918

hydrogens, with a carbon−hydrogen distance of 1.093 Å. The C_{60} is displaced perpendicular to the tube so as to match the DFT SWCNT/C_{60} minimum energy distance of 3 Å obtained with LC-ωPBE/6-31G* and the XDM dispersion model[31,32] to within ±0.15 Å. The potential energy curves for the intermolecular interaction of the C_{60} and SWCNT fragment obtained with LC-ωPBE-XDM and the AIREBO potential are in excellent agreement (see Figure S4).

We computed the band structure of C_{60} adsorbed on SWCNTs of the three different chiralities with DFT and the 6-31G* basis set as implemented in the TeraChem electronic structure package (http://www.petachem.com).[33−36] Results using the B3LYP hybrid functional[37,38] are shown in Figure 5,

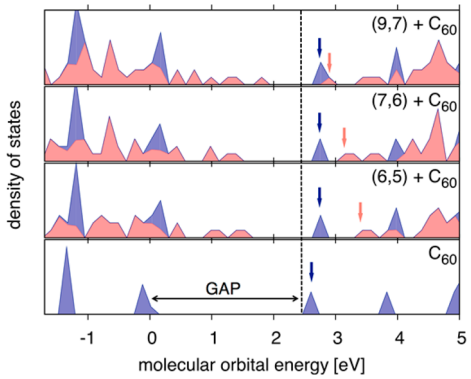

Figure 5. Projected B3LYP DFT density of states for C_{60} and C_{60} adsorbed onto (9,7), (7,6), and (6,5) SWCNTs. The C_{60} energy levels are blue, the SWCNT energy levels are light-red. Lowest-energy empty orbitals that have dominant C_{60} and SWCNT contributions are indicated with vertical arrows. The dashed line marks the edge of the conduction band.

with contributions from C_{60} in dark-blue and SWCNTs in light-red. All energies were shifted by 6.0 eV to place the isolated C_{60} valence band edge at 0.0 eV. Because the molecular orbital energies of adsorbed C_{60} are similar to those of C_{60} in isolation, the electronic structure of C_{60} is not strongly affected by interaction with the SWCNT, based on this single-particle picture.

The key result for rationalizing the difference in photocurrents is the placement of the conduction band energy levels of C_{60} relative to the conduction band energy levels of the SWCNTs, indicated with vertical arrows in Figure 5. For the (9,7), (7,6), and (6,5) SWCNT chiralities studied here, the SWCNT has lowest-energy conduction band levels (light-red arrows) at higher energies than those of the fullerene (dark-blue arrows). The energy gap between these electron-acceptor levels provides the driving force for exciton dissociation, with the excited electron transferring from the SWCNT to the adsorbed fullerene. If the energy gap is small, the separated excited electron and hole will remain on the SWCNT and easily recombine. If the energy gap is large, the electron will transfer from the SWCNT to the fullerene, leading to charge separation. Our calculations predict that the energy gap increases in the order (9,7) < (7,6) < (6,5). This trend directly correlates with the amount of electric current produced (Figure 1). Note that the B3LYP functional performs quite well in computing SWCNT band gaps,[39] but similar relative energetics of the conduction band edge were calculated with the BLYP and LC-ωPBE[40] functionals; these results are available in the SI.

In conclusion, we have shown that the chirality of the SWCNT is key to controlling the charge transfer efficiency in nanocarbon SWCNT/C_{60} hybrid photovoltaics. For the three SWCNT chiralities studied, our experimental and theoretical results demonstrate that the likelihood of exciton separation and charge transfer from the SWCNT to C_{60} increases in the order (9,7) < (7,6) < (6,5). DFT band structure calculations indicate that this ordering is due to the relative gaps in the SWCNT and C_{60} conduction band levels. Charge separation can be optimized by choosing a SWCNT with a conduction band higher in energy than that of C_{60}, thus providing an energetic driving force for separation of the electron−hole pair and increasing the efficiency of the charge transfer. The approach presented here combines a variety of nanocarbon constituents in a strategic manner in order to optimize electron transfer; we hope that this technique will provide the first steps to constructing high-performing all-carbon-based photoconductive devices.

■ ASSOCIATED CONTENT

Supporting Information

A description of the synthesis of the graphene nanoribbon surfactants, atomic force microscopy image, data for the device without the PCBM layer, a plot of the LC-ωPBE-XDM and the AIREBO C_{60}-SWCNT potential energy surface, BLYP and LC-ωPBE density of states plots for C_{60} adsorbed onto (9,7), (7,6), and (6,5) SWCNTs, and the corresponding Cartesian coordinates. This material is available free of charge via the Internet at http://pubs.acs.org

■ AUTHOR INFORMATION

Corresponding Author

*E-mail: cisborn@ucmerced.edu (C.M.I.); ctung@ucmerced.edu (V.C.T.).

Author Contributions

The manuscript was written through contributions of all authors. All authors have given approval to the final version of the manuscript.

Notes

The authors declare no competing financial interest.

■ ACKNOWLEDGMENTS

We greatly appreciate help from Jaemung Kim, Tejas Shastry, Professor Jiaxing Huang, and Professor Mark C. Hersam for purification of SWCNTs and Dr. Gang Li and Professor Yang Yang for providing ZnO nanoparticles. Some of the imaging was performed at the NUANCE center at Northwestern University and at Lawrence Berkeley National Laboratory through the Molecular Foundry (Proposal #1755) with the help of Teresa Chen. AOR thanks the Spanish Malta/Consolider initiative (no. CSD 2007-00045).

■ REFERENCES

(1) Graetzel, M.; Janssen, R. A. J.; Mitzi, D. B.; Sargent, E. H. Materials Interface Engineering for Solution-Processed Photovoltaics. *Nature* **2012**, *488*, 304−312.

(2) Nelson, J. Polymer:Fullerene Bulk Heterojunction Solar Cells. *Mater. Today* **2011**, *14*, 462−470.

(3) Arnold, M. S.; Zimmerman, J. D.; Renshaw, C. K.; Xu, X.; Lunt, R. R.; Austin, C. M.; Forrest, S. R. Broad Spectral Response Using Carbon Nanotube/Organic Semiconductor/C_{60} Photodetectors. *Nano Lett.* **2009**, *9*, 3354−3358.

(4) Jain, R. M.; Howden, R.; Tvrdy, K.; Shimizu, S.; Hilmer, A. J.; McNicholas, T. P.; Gleason, K. K.; Strano, M. S. Polymer-Free Near-Infrared Photovoltaics with Single Chirality (6,5) Semiconducting Carbon Nanotube Active Layers. *Adv. Mater.* **2012**, *24*, 4436−4439.
(5) Ramuz, M. P.; Vosgueritchian, M.; Wei, P.; Wang, C.; Gao, Y.; Wu, Y.; Chen, Y.; Bao, Z. Evaluation of Solution-Processable Carbon-Based Electrodes for All-Carbon Solar Cells. *ACS Nano* **2012**, *6*, 10384−10395.
(6) Ren, S.; Bernardi, M.; Lunt, R. R.; Bulovic, V.; Grossman, J. C.; Gradečak, S. Toward Efficient Carbon Nanotube/P3HT Solar Cells: Active Layer Morphology, Electrical, and Optical Properties. *Nano Lett.* **2011**, *11*, 5316−5321.
(7) Tung, V. C.; Huang, J.-H.; Kim, J.; Smith, A. J.; Chu, C.-W.; Huang, J. Towards Solution Processed All-Carbon Solar Cells: A Perspective. *Energy Environ. Sci.* **2012**, *5*, 7810−7818.
(8) Tung, V. C.; Huang, J.-H.; Tevis, I.; Kim, F.; Kim, J.; Chu, C.-W.; Stupp, S. I.; Huang, J. Surfactant-Free Water-Processable Photoconductive All-Carbon Composite. *J. Am. Chem. Soc.* **2011**, *133*, 4940−4947.
(9) Bernardi, M.; Lohrman, J.; Kumar, P. V.; Kirkeminde, A.; Ferralis, N.; Grossman, J. C.; Ren, S. Nanocarbon-Based Photovoltaics. *ACS Nano* **2012**, *6*, 8896−8903.
(10) Umeyama, T.; Imahori, H. Photofunctional Hybrid Nanocarbon Materials. *J. Phys. Chem. C* **2012**, *117*, 3195−3209.
(11) Umeyama, T.; Baek, J.; Tezuka, N.; Morita, K.; Imahori, H. Incorporation of Graphene to Fullerene Clusters and Fullerene-Nanotube Composites and Their Photoelectrochemical Properties. *ECS J. Solid State Sci. Technol.* **2013**, *2*, M3001−M3007.
(12) Guldi, D. M.; Costa, R. D. Nanocarbon Hybrids: The Paradigm of Nanoscale Self-Ordering/Self-Assembling by Means of Charge Transfer/Doping Interactions. *J. Phys. Chem. Lett.* **2013**, *4*, 1489−1501.
(13) Martín, N.; Sánchez, L.; Illescas, B.; Pérez, I. C_{60}-Based Electroactive Organofullerenes. *Chem. Rev.* **1998**, *98*, 2527−2548.
(14) Echegoyen, L.; Echegoyen, L. E. Electrochemistry of Fullerenes and Their Derivatives. *Acc. Chem. Res.* **1998**, *31*, 593−601.
(15) Guldi, D. M. Fullerene-porphyrin Architectures; Photosynthetic Antenna and Reaction Center Models. *Chem. Soc. Rev.* **2002**, *31*, 22−36.
(16) Bottari, G.; de la Torre, G.; Guldi, D. M.; Torres, T. Covalent and Noncovalent Phthalocyanine−Carbon Nanostructure Systems: Synthesis, Photoinduced Electron Transfer, and Application to Molecular Photovoltaics. *Chem. Rev.* **2010**, *110*, 6768−6816.
(17) Sariciftci, N. S.; Smilowitz, L.; Heeger, A. J.; Wudl, F. Photoinduced Electron Transfer from a Conducting Polymer to Buckminsterfullerene. *Science* **1992**, *258*, 1474−1476.
(18) Imahori, H. Creation of Fullerene-Based Artificial Photosynthetic Systems. *Bull. Chem. Soc. Jpn.* **2007**, *80*, 621−636.
(19) Imahori, H.; Umeyama, T. Donor−Acceptor Nanoarchitecture on Semiconducting Electrodes for Solar Energy Conversion. *J. Phys. Chem. C* **2009**, *113*, 9029−9039.
(20) Beaujuge, P. M.; Fréchet, J. M. J. Molecular Design and Ordering Effects in π-Functional Materials for Transistor and Solar Cell Applications. *J. Am. Chem. Soc.* **2011**, *133*, 20009−20029.
(21) Cai, W.; Zhu, Y.; Li, X.; Piner, R. D.; Ruoff, R. S. Large Area Few-layer Graphene/Graphite Films as Transparent Thin Conducting Electrodes. *App. Phys. Lett.* **2009**, *95*, 123115−123113.
(22) Li, X.; Wang, X.; Zhang, L.; Lee, S.; Dai, H. Chemically Derived, Ultrasmooth Graphene Nanoribbon Semiconductors. *Science* **2008**, *319*, 1229−1232.
(23) Kosynkin, D. V.; Higginbotham, A. L.; Sinitskii, A.; Lomeda, J. R.; Dimiev, A.; Price, B. K.; Tour, J. M. Longitudinal Unzipping of Carbon Nanotubes to Form Graphene Nanoribbons. *Nature* **2009**, *458*, 872−876.
(24) Tang, C.; Oppenheim, T.; Tung, V. C.; Martini, A. Structure−Stability Relationships for Graphene-Wrapped Fullerene-Coated Carbon Nanotubes. *Carbon* **2013**, *61*, 458−466.
(25) Li, S.-S.; Tu, K.-H.; Lin, C.-C.; Chen, C.-W.; Chhowalla, M. Solution-Processable Graphene Oxide as an Efficient Hole Transport Layer in Polymer Solar Cells. *ACS Nano* **2010**, *4*, 3169−3174.
(26) Gao, Y.; Yip, H.-L.; Hau, S. K.; O'Malley, K. M.; Cho, N. C.; Chen, H.; Jen, A. K. Y. Anode Modification of Inverted Polymer Solar Cells Using Graphene Oxide. *Appl. Phys. Lett.* **2010**, *97*, 203306−203303.
(27) Tung, V. C.; Kim, J.; Huang, J. Graphene Oxide:Single-Walled Carbon Nanotube-Based Interfacial Layer for All-Solution-Processed Multijunction Solar Cells in Both Regular and Inverted Geometries. *Adv. Energy Mater.* **2012**, *2*, 299−303.
(28) Tanaka, Y.; Hirana, Y.; Niidome, Y.; Kato, K.; Saito, S.; Nakashima, N. Experimentally Determined Redox Potentials of Individual (*n*,*m*) Single-Walled Carbon Nanotubes. *Angew. Chem., Int. Ed.* **2009**, *48*, 7655−7659.
(29) Stuart, S. J.; Tutein, A. B.; Harrison, J. A. A Reactive Potential for Hydrocarbons with Intermolecular Interactions. *J. Chem. Phys.* **2000**, *112*, 6472−6486.
(30) Plimpton, S. Fast Parallel Algorithms for Short-Range Molecular Dynamics. *J. Comput. Phys.* **1995**, *117*, 1−19.
(31) Otero-de-la-Roza, A.; Johnson, E. R. Van der Waals Interactions in Solids Using the Exchange-Hole Dipole Moment Model. *J. Chem. Phys.* **2012**, *136*, 174109−174108.
(32) Otero-de-la-Roza, A.; Johnson, E. R. Non-covalent Interactions and Thermochemistry Using XDM-Corrected Hybrid and Range-Separated Hybrid Density Functionals. *J. Chem. Phys.* **2013**, *138*, 204109−204113.
(33) Ufimtsev, I. S.; Martinez, T. J. Quantum Chemistry on Graphical Processing Units. 1. Strategies for Two-Electron Integral Evaluation. *J. Chem. Theory Comput.* **2008**, *4*, 222−231.
(34) Ufimtsev, I. S.; Martinez, T. J. Quantum Chemistry on Graphical Processing Units. 2. Direct Self-Consistent-Field Implementation. *J. Chem. Theory Comput.* **2009**, *5*, 1004−1015.
(35) Ufimtsev, I. S.; Martinez, T. J. Quantum Chemistry on Graphical Processing Units. 3. Analytical Energy Gradients, Geometry Optimization, and First Principles Molecular Dynamics. *J. Chem. Theory Comput.* **2009**, *5*, 2619−2628.
(36) Isborn, C. M.; Luehr, N.; Ufimtsev, I. S.; Martinez, T. J. Excited-State Electronic Structure with Configuration Interaction Singles and Tamm−Dancoff Time-Dependent Density Functional Theory on Graphical Processing Units. *J. Chem. Theory Comput.* **2011**, *7*, 1814−1823.
(37) Becke, A. D. Density-Functional Exchange-Energy Approximation with Correct Asymptotic Behavior. *Phys. Rev. A* **1988**, *38*, 3098−3100.
(38) Lee, C.; Yang, W.; Parr, R. G. Development of the Colle−Salvetti Correlation-Energy Formula into a Functional of the Electron Density. *Phys. Rev. B* **1988**, *37*, 785−789.
(39) Matsuda, Y.; Tahir-Kheli, J.; Goddard, W. A. Definitive Band Gaps for Single-Wall Carbon Nanotubes. *J. Phys. Chem. Lett.* **2010**, *1*, 2946−2950.
(40) Vydrov, O. A.; Scuseria, G. E. Assessment of a Long-Range Corrected Hybrid Functional. *J. Chem. Phys.* **2006**, *125*, 234109.